Plasmon dispersion relations and the induced electron interaction in oxide superconductors: Numerical results

A. Griffin and A. J. Pindor*
Department of Physics, University of Toronto, Toronto, Ontario Canada M5S 1A7
(Received 1 February 1989)

Recently it is been argued that the plasmon modes expected in the oxide superconductors should be characteristic of a superlattice with a basis of several metallic sheets. We extend this work by including the exchange-correlation effects in a given CuO sheet via local-field corrections (the generalized random-phase approximation). In addition, the effective interaction between electrons in a given CuO sheet is worked out for a superlattice with a basis of several sheets, separating out the effects of the various kinds of plasmons. Numerical results are given for the superlattice plasmon dispersion relations for two and three sheets/unit cell. If the spacing of the sheets is small compared to the superlattice period (as it is in the 2:2:1:2 and 2:2:2:3 superconductors), we find that the low-frequency plasmon branches ($n-1$ of them, where n is the number of sheets/unit cell) are essentially identical to those of an isolated bilayer or trilayer.

I. INTRODUCTION

This paper is concerned with the plasmon spectrum which should be characteristic of the Bi-Sr-Ca-Cu-O and Tl-Ba-Ca-Cu-O high-temperature superconductors. As the result of experimental work by many groups since the original report of Maeda *et al.*,[1] it is now known that there is a whole class of oxide superconductors composed of monolayer, bilayer, or trilayer Cu-perovskitelike units separated by bilayer Bi-O or Tl-O units (see, for example, Refs. 2–6). These superconductors can be described by the formulas $Bi_2Sr_2Ca_{n-1}Cu_nO_{4+2n}$ and $Tl_2Ba_2Ca_{n-1}Cu_nO_{4+2n}$, where $2n$ is the number of CuO_2 sheets in a primitive lattice unit cell with a c-axis dimension $c_L(n)$. From several band-structure studies,[7–9] the metallic properties appear to be dominated by two-dimensional (2D) bands associated with the CuO_2 sheets and (possibly) the Bi_2O_2 (Tl_2O_2) bilayers, with not very significant charge transfer between these subunits. The layers with Ca and Sr(Ba) do not appear to exhibit metalliclike behavior. In this paper, in discussing the charge fluctuation spectra of this class of materials, we treat them as a superlattice of stacked metallic sheets (2D electron gases), with a superlattice unit cell with a c-axis period (along the z axis) equal to one half of the crystal unit cell ($c=c_L/2$). Each superlattice unit cell has one Bi-O(Tl-O) bilayer and n CuO_2 sheets ($n=1,2,3,\ldots$).

Starting with such a superlattice with a complex unit cell composed of several metallic sheets, the dielectric function $\epsilon(\mathbf{q},\omega)$ was worked out in Refs. 10 and 11 within the random-phase approximation (RPA) for a basis of up to three sheets/unit cell. Extending earlier work[12] in semiconductor superlattices with two sheets per unit cell, for n metallic sheets per unit cell, one has $n-1$ low-energy acoustic plasmon branches which separate off from the high-energy plasmon branch characteristic[13] of a superlattice with one sheet/unit cell.

In the present paper, we generalize our earlier work[11] in several ways. First of all, we generalize the analysis of the charge fluctuations in a given sheet to include the exchange-correlation effects via a static local-field approximation.[14] That is, we extend our analysis to the generalized RPA (GRPA), albeit in a simple Hubbard-like approximation.[15] As far as we are aware, the only previous work on including exchange-correlation corrections to the superlattice plasmon dispersion relation was limited[16] to the long-wavelength limit. Second, we derive a general expression for the effective Coulomb interaction between electrons in a given CuO_2 sheet, as induced by coupling into the superlattice charge fluctuation spectrum. We give a closed expression for the effective electron-electron interaction in a given sheet in terms of separate contributions from the high- and low-frequency plasmon branches $\omega_\pm$ in a superlattice with two identical sheets/unit cell. This makes use of the fact that the dielectric function can be factorized into separate parts associated with the $\omega_\pm$ plasmons, and generalizes an earlier study on superlattices *without* a basis.[17]

In addition, we present numerical results for the plasmon dispersion relations in superlattices with two and three sheets/unit cell. We find that as long as the spacing d_1 of the sheets is much smaller than the period of the superlattice c (as in the Bi and Tl superconductors), the low-energy plasmons are almost identical to that of an isolated bilayer or trilayer.

Direct observation of these superlattice plasmon modes would be of great interest since their dispersion relations depend on the spacing and metallic properties of the sheets. In the oxide superconductors, the bulk plasmon frequency is of order 1–2 eV. In addition, if the Bi_2O_2 and Tl_2O_2 bilayers are metallic (as band-structure studies suggest), they would give rise to an additional low-energy acoustic plasmon branch.[11] Such superlattice plasmons have been extensively studied in semiconductors (for a re-

view, see Ref. 18) by inelastic scattering of light. In the oxide superlattices, the ideal probe of the low-energy plasmons would appear to be inelastic electron scattering in the reflection mode.

In Sec. II, we work out the charge-fluctuation-induced electron-electron interaction for the case of two sheets/unit cell, within the RPA. In Sec. III, we generalize the analysis to the GRPA. In Sec. IV, working in the RPA and the long-wavelength limit, we discuss the plasmon branches arising when the basis has one, two, and three sheets. In Sec. V, we give numerical results for the superlattice plasmon dispersion relations for two and three sheets/unit cell, as well as the associated effective electron interaction. In Sec. VI, we briefly discuss recent work on Cooper pairing due to acoustic plasmons in a single two-dimensional (2D) metallic sheet[19] as well as in an isolated bilayer[20] or trilayer.[21] In a future paper, we hope to use our present results to give a more definitive test of plasmon-induced pairing in the oxide superconductors.

II. PLASMON-INDUCED EFFECTIVE ELECTRON INTERACTION IN A SUPERLATTICE WITH A BASIS OF TWO SHEETS: RPA

In the present paper, we completely ignore any band-structure effects in the CuO_2 and Bi_2O_2 (Tl_2O_2) bilayers and simply treat these as 2D electron gases (with different densities and effective masses). We completely ignore charge transfer between the sheets, which should be a good assumption in view of the highly 2D nature[7-10] of the energy bands that cross (or are near) the Fermi energy. This simplifies the analysis considerably and should be an appropriate first approximation to the extent that the width of the electronic charge density in a given sheet is much less than the c, the superlattice repeat distance. This means that all the sheet form factors in our earlier work[11] are set to unity [$\beta_s(q_z)=1$].

Our starting point is the self-consistent RPA equation for the effective electron-electron interaction (between electrons in cells labeled by l and l')

$$v_{ij}^{\rm eff}(l,l';\mathbf{q}_\parallel,\omega)=v_{ij}(l-l';\mathbf{q}_\parallel)+\frac{1}{c}\sum_{j_1,l_1}v_{ij_1}(l-l_1,q_\parallel)\chi_{j_1}^0(l=0;q_\parallel,\omega)v_{j_1j}^{\rm eff}(l_1,l';\mathbf{q}_\parallel,\omega)\,. \tag{2.1}$$

The indices i,j label the two metallic sheets (a and b) in given unit cell. The bare Coulomb interaction is

$$v_{ij}(l-l';\mathbf{q}_\parallel)=\frac{2\pi e^2}{q_\parallel}ce^{-q_\parallel|Z_{l,i}-Z_{l'j}|}\,, \tag{2.2}$$

where $Z_{l,a}=lc$ and $Z_{l,b}=lc+d_1$; l is an integer running over the N unit cells in the superlattice. We have assumed that sheet a is at $z_a=0$ and sheet b is at $z_b=d_1$. The general charge response function describing the correlation between electrons in sheet i in unit cell l, and in sheet j in unit cell l' would be denoted as $\chi_{ij}(l,l';\mathbf{q}_\parallel,\omega)$. For noninteracting electrons, this response function is diagonal, with $\chi_{ii}^0(l,l;\mathbf{q}_\parallel,\omega)\equiv\chi_i^0(l'=0;\mathbf{q}_\parallel,\omega)$. From now on, we shall drop the $\mathbf{q}_\parallel,\omega$ dependence of various functions to simplify the notation. If we limit ourselves to a single sheet/unit cell, (2.1) reduces to the self-consistent equation discussed in Ref. 17.

In solving (2.1), it is convenient to use Fourier transforms with respect to l and l' to make use of the periodicity in the z direction. For example, the Fourier transform of (2.2) is (compare with Ref. 11)

$$v_{ij}(q_z)=\sum_l e^{iq_zlc}v_{ij}(l)\,. \tag{2.3}$$

Here G_z is a reciprocal-lattice vector of the superlattice ($=n2\pi/c$). Because of the periodicity in the z direction, q_z is restricted to the first Brillouin zone ($-\pi/c<q_z<\pi/c$). For later purposes, we note that the sum in (2.3) can be carried out explicitly to give

$$v_{aa}(\mathbf{q})=v_{bb}(\mathbf{q})=\tilde{v}(\mathbf{q})=\sum_{G_z}\frac{4\pi e^2}{q_\parallel^2+(q_z+G_z)^2}\,, \tag{2.4}$$

$$v_{ab}(\mathbf{q})=v_{ba}^*(\mathbf{q})=\bar{v}(\mathbf{q})=\sum_{G_z}\frac{4\pi e^2}{q_\parallel^2+(q_z+G_z)^2}e^{-i(G_z)d_1}\,, \tag{2.5}$$

where[11,13]

$$\tilde{v}(\mathbf{q})=\frac{2\pi e^2}{q_\parallel}c\left(\frac{\sinh q_\parallel c}{\cosh q_\parallel c-\cos q_z c}\right),$$

$$\bar{v}(\mathbf{q})=\frac{2\pi e^2}{q_\parallel}c\left(\frac{\sinh q_\parallel(c-d_1)+e^{-iq_zc}\sinh q_\parallel d_1}{\cosh q_\parallel c-\cos q_z c}\right)e^{iq_zd_1}. \tag{2.6}$$

In the limit of $qc\ll 1$, one finds $\tilde{v}(\mathbf{q})=\bar{v}(\mathbf{q})=4\pi e^2/q^2$. The Fourier-transform convention in this paper is slightly different from Ref. 11. In particular, the transform of $x_{aa}^0(l,l')$ is

$$\frac{1}{c}\chi_{aa}^0(q_z)=\frac{1}{c}\chi_a^0(l-l'=0)=N_s\chi_a^0(\mathbf{q}_\parallel,\omega)\,, \tag{2.7}$$

where $N_s=1/Ac$ is the number of unit cells per unit volume and $\chi_a^0(\mathbf{q}_\parallel,\omega)$ is the Lindhard function of a 2D electron gas. A is the area of a sheet. An overall phase factor is corrected in (2.5) and (2.6).

Fourier transforming (2.1), we obtain

$$v_{aa}^{\rm eff}(\mathbf{q})=\tilde{v}(\mathbf{q})+N_s\chi_a^0(\mathbf{q}_\parallel,\omega)\tilde{v}(\mathbf{q})v_{aa}^{\rm eff}(\mathbf{q})+N_s\chi_b^0(\mathbf{q}_\parallel,\omega)\bar{v}(\mathbf{q})v_{ba}^{\rm eff}(\mathbf{q})\,, \tag{2.8a}$$

$$v_{ba}^{\rm eff}(\mathbf{q})=\bar{v}^*(\mathbf{q})+N_s\chi_a^0(\mathbf{q}_\parallel,\omega)\bar{v}^*(\mathbf{q})v_{aa}^{\rm eff}(\mathbf{q})+N_s\chi_b^0(\mathbf{q}_\parallel,\omega)\tilde{v}(\mathbf{q})v_{ba}^{\rm eff}(\mathbf{q})\,. \tag{2.8b}$$

This is a closed set of equations whose solution is

$$v_{aa}^{\rm eff}(\mathbf{q})=\frac{\tilde{v}(\mathbf{q})-[\tilde{v}^2(\mathbf{q})-|\bar{v}(\mathbf{q})|^2]N_s\chi_b^0}{\epsilon}\,,$$

$$v_{ba}^{\rm eff}(\mathbf{q})=\frac{\bar{v}^*(\mathbf{q})}{\epsilon}\,, \tag{2.9}$$

where the superlattice dielectric function is given by

$$\epsilon\equiv\epsilon_a\epsilon_b-|\bar{v}(\mathbf{q})|^2N_s\chi_a^0N_s\chi_b^0 \tag{2.10}$$

and

$$\epsilon_i \equiv 1 - N_s \tilde{v}(\mathbf{q}) \chi_i^0(\mathbf{q}_\parallel, \omega) , \quad i = a,b . \tag{2.11}$$

Analogous calculations give

$$v_{bb}^{\text{eff}}(\mathbf{q}) = \frac{\tilde{v}(\mathbf{q}) - [\tilde{v}^2(\mathbf{q}) - |\bar{v}(\mathbf{q})|^2] N_s \chi_a^0}{\epsilon} ,$$

$$v_{ab}^{\text{eff}}(\mathbf{q}) = \frac{\bar{v}(\mathbf{q})}{\epsilon} . \tag{2.12}$$

We note that while $\tilde{v}$ in (2.4) only depends on the Bravais superlattice spacing c, $\bar{v}$ in (2.5) also depends on the structure of the basis. If we set $\bar{v}$ to zero, the above results describe two *uncoupled* arrays, with $\epsilon = \epsilon_a \epsilon_b$ and[17]

$$v_{ij}^{\text{eff}}(\mathbf{q}) = \frac{\tilde{v}(\mathbf{q})}{\epsilon_i} \delta_{ij} . \tag{2.13}$$

The charge-fluctuation spectrum is given by the zeros of ϵ in (2.10) and the resulting plasmon dispersion relations will be discussed in Secs. IV and V. The effective interaction between electrons in specific sheets is given by

$$v_{ij}^{\text{eff}}(l - l'; \mathbf{q}_\parallel, \omega) = \left(\frac{1}{N} \right) \sum_{q_z} e^{i q_z (l - l')_c} v_{ij}^{\text{eff}}(q_z, \mathbf{q}_\parallel, \omega) , \tag{2.14}$$

where q_z is restricted to the first BZ of the superlattice (the spacing between the q_z wave vectors is $2\pi/L$, where $L = Nc$). In the continuum limit, the intrasheet effective electron-electron interaction is

$$v_{aa}^{\text{eff}}(l - l' = 0; \mathbf{q}_\parallel, \omega) = \frac{c}{2\pi} \int_{-\pi/c}^{\pi/c} dq_z \, v_{aa}^{\text{eff}}(\mathbf{q}) , \tag{2.15}$$

while the effective interaction between electrons in different sheets in the same unit cell is

$$v_{ba}^{\text{eff}}(l - l' = 0; \mathbf{q}_\parallel, \omega) = \frac{c}{2\pi} \int_{-\pi/c}^{\pi/c} dq_z \, v_{ba}^{\text{eff}}(\mathbf{q}) . \tag{2.16}$$

If we consider the $c \to \infty$ limit, the different cells are uncoupled and our results in (2.9)–(2.12) then describe an isolated bilayer.[22] In this limit, the potentials in (2.6) are[11,23]

$$\tilde{v} = v_{2D} , \quad \bar{v}(d_1) = v_{2D} e^{-q_\parallel d_1 + i q_z d_1} , \tag{2.17}$$

where $v_{2D} \equiv 2\pi e^2 c / q_\parallel$. The effective potentials in (2.9) and (2.12) then reduce to those recently obtained by Mahan and Wu[21] for the case of an isolated bilayer. For a single sheet, (2.15) gives the standard RPA results (see, for example, Ref. 19).

In Appendix A, we briefly discuss the generalization of the results in this section for a superlattice basis of three sheets.

III. INCLUSION OF EXCHANGE AND CORRELATION: GRPA

We now proceed to generalize the RPA results of Sec. II to include exchange and correlation effects through the use of static-local-field corrections in describing the Coulomb interactions in a given sheet. This has been discussed extensively in bulk 3D metallic systems,[15] as well as for 2D systems,[14] and we refer the reader to this literature for further background on the GRPA.

Our key assumption is that in a superlattice, only the intrasheet Coulomb interaction is renormalized by local-field corrections:

$$v_{ij}'(l,l';\mathbf{q}_\parallel) \equiv v_{ij}(l,l';\mathbf{q}_\parallel) - G_i(\mathbf{q}_\parallel) v_{2D}(\mathbf{q}_\parallel) \delta_{l,l'} \delta_{ij} . \tag{3.1}$$

A simple Hubbard-like approximation to the 2D static local-field correction which has the correct limits is[14,19]

$$G(\mathbf{q}_\parallel) = \frac{q_\parallel}{[(2q_\parallel)^2 + (\pi k_{2F})^2]^{1/2}} , \tag{3.2}$$

where k_{2F} is the 2D Fermi momentum. This reduces to $\frac{1}{2}$ for $q_\parallel \gg k_{2F}$ and $q_\parallel / \pi k_{2F}$ for $q_\parallel \ll k_{2F}$. With reference to the superlattice potentials in Sec. II, we note that $\tilde{v}(\mathbf{q})$ will be modified but $\bar{v}(\mathbf{q})$ will be unaffected since the latter describes interactions between different sheets in the basis. v_{2D} has been defined after Eq. (2.17).

The effective interaction is now given by

$$v_{ij}^{\text{eff}}(l,l') = v_{ij}(l - l') + \frac{1}{c} \sum_{j_1, l_1} v_{ij_1}'(l - l_1) \chi_{j_1}^0(l = 0) \bar{v}_{j_1,j}^{\text{eff}}(l_1, l') , \tag{3.3}$$

where v_{ij}' is defined in (3.1) and $\bar{v}^{\text{eff}}$ satisfies the self-consistent equation

$$\bar{v}_{ij}^{\text{eff}}(l,l') = v_{i,j}'(l - l') + \frac{1}{c} \sum_{j_1, l_1} v_{ij_1}'(l - l_1) \chi_{j_1}^0(l = 0) \bar{v}_{j_1,j}^{\text{eff}}(l_1, l') . \tag{3.4}$$

The lowest-order term in (3.3) is the bare or unscreened Coulomb potential while the higher-order terms involve v_{ij}'. Fourier transforming (3.4), one finds $\bar{v}_{aa}^{\text{eff}}$ and $\bar{v}_{ba}^{\text{eff}}$ satisfy a set of equations identical to (2.8) except that $\tilde{v}(\mathbf{q})$ is replaced by

$$\tilde{v}_a'(\mathbf{q}) \equiv \tilde{v}(\mathbf{q}) - v_{2D}(\mathbf{q}_\parallel) G_a(\mathbf{q}_\parallel) \tag{3.5}$$

in (2.8a) and by $\tilde{v}_b'(\mathbf{q})$ in (2.8b). The solutions are

$$\bar{v}_{aa}^{\text{eff}}(\mathbf{q}) = \frac{\tilde{v}_a'(\mathbf{q}) \epsilon_b' + |\bar{v}(\mathbf{q})|^2 N_s \chi_b^0}{\epsilon'} ,$$

$$\bar{v}_{ba}^{\text{eff}}(\mathbf{q}) = \frac{\bar{v}^*(\mathbf{q})}{\epsilon'} , \tag{3.6}$$

with

$$\epsilon' \equiv \epsilon_a' \epsilon_b' - |\bar{v}(\mathbf{q})|^2 N_s \chi_a^0 N_s \chi_b^0 , \tag{3.7}$$

and

$$\epsilon_i'(\mathbf{q}, \omega) = 1 - [\tilde{v}(q) - G_i v_{2D}] N_s \chi_i^0(\mathbf{q}_\parallel, \omega) , \quad i = a,b . \tag{3.8}$$

Turning to (3.3), the Fourier transform is

$$\begin{aligned} v_{aa}^{\text{eff}}(\mathbf{q}) &= \tilde{v}(\mathbf{q}) + N_s \chi_a^0(\mathbf{q}_\parallel) \tilde{v}_a'(\mathbf{q}) \bar{v}_{aa}^{\text{eff}}(\mathbf{q}) \\ &\quad + N_s \chi_b^0(\mathbf{q}_\parallel) \bar{v}(\mathbf{q}) \bar{v}_{ba}^{\text{eff}}(\mathbf{q}) , \\ v_{ba}^{\text{eff}}(\mathbf{q}) &= \bar{v}^*(\mathbf{q}) + N_s \chi_a^0(\mathbf{q}_\parallel) \bar{v}^*(\mathbf{q}) \bar{v}_{aa}^{\text{eff}}(\mathbf{q}) \\ &\quad + N_s \chi_b^0(\mathbf{q}_\parallel) \tilde{v}_b'(\mathbf{q}) \bar{v}_{ba}^{\text{eff}}(\mathbf{q}) . \end{aligned} \tag{3.9}$$

Making use of (3.6) in (3.9), we obtain

$$v_{aa}^{\rm eff}(\mathbf{q},\omega)=\tilde{v}(\mathbf{q})+[N_s\chi_a^0(\tilde{v}_a')^2+N_s\chi_b^0|\bar{v}|^2+N_s\chi_a^0N_s\chi_b^0\tilde{v}_a'(|\bar{v}|^2-\tilde{v}_a'\tilde{v}_b')]/\epsilon' . \tag{3.10}$$

For one sheet/unit cell, this simplifies to

$$v_{aa}^{\rm eff}(\mathbf{q},\omega)=\tilde{v}(q)+(\tilde{v}_a')^2\frac{N_s\chi_a^0(\mathbf{q}_\parallel,\omega)}{1-\tilde{v}_a'(\mathbf{q})N_s\chi_a^0(\mathbf{q}_\parallel,\omega)} . \tag{3.11}$$

If we ignore the local-field correction $G_a(\mathbf{q}_\parallel)$, this in turn reduces to $\tilde{v}/\epsilon_a$ as in (2.13).

For the special case of two identical sheets, we note that we can write the dielectric function in (3.7) as a product of two factors $\epsilon'=\epsilon_+'\epsilon_-'$, where we have defined

$$\epsilon_\pm'=1-v_\pm' N_s\chi^0(\mathbf{q}_\parallel,\omega) , \tag{3.12}$$

with

$$v_\pm'\equiv\tilde{v}'\pm|\bar{v}|=v_\pm-G(\mathbf{q}_\parallel)v_{2D} \tag{3.13}$$

In this case of two identical sheets, (3.6) simplifies to

$$\begin{aligned}\bar{v}_{aa}^{\rm eff}(\mathbf{q},\omega)&=\frac{\tilde{v}'-(\tilde{v}'^2-|\bar{v}|^2)N_s\chi^0}{\epsilon}\\&=\frac{v_+'+v_-'-2v_+'v_-'N_s\chi^0}{2\epsilon_+'\epsilon_-'}\\&=\frac{v_+'\epsilon_-'+v_-'\epsilon_+'}{2\epsilon_+'\epsilon_-'}\\&=\frac{v_+'}{2\epsilon_+'}+\frac{v_-'}{2\epsilon_-'} .\end{aligned} \tag{3.14}$$

This neatly separates the effect of the two kinds of plasmons $\omega_\pm'$ (zeros of $\epsilon_\pm'$) on $\bar{v}_{aa}^{\rm eff}$. Similarly, one may show

$$\bar{v}_{ba}^{\rm eff}(\mathbf{q},\omega)=\frac{\bar{v}^*}{2|\bar{v}|N_s\chi^0}\left(\frac{1}{\epsilon_+'}-\frac{1}{\epsilon_-'}\right) . \tag{3.15}$$

Using (3.13) and (3.14) in (3.9), we find

$$\begin{aligned}v_{aa}^{\rm eff}(\mathbf{q},\omega)=\tilde{v}&+\frac{1}{2\epsilon_+'}[N_s\chi^0(\tilde{v}')^2+|\bar{v}|(1+N_s\chi^0\tilde{v}')]\\&+\frac{1}{2\epsilon_-'}[N_s\chi^0(\tilde{v}')^2-|\bar{v}|(1+N_s\chi^0\tilde{v}')] .\end{aligned} \tag{3.16}$$

Splitting up the first term as

$$\tilde{v}=\frac{1}{2}\tilde{v}\frac{\epsilon_+'}{\epsilon_+'}+\frac{1}{2}\tilde{v}\frac{\epsilon_-'}{\epsilon_-'} , \tag{3.17}$$

one is finally able to reduce (3.16) to

$$\begin{aligned}v_{aa}^{\rm eff}(\mathbf{q},\omega)=&\frac{1}{2\epsilon_+'}[v_+-v_+'G(\mathbf{q}_\parallel)v_{2D}N_s\chi^0]\\&+\frac{1}{2\epsilon_-'}[v_--v_-'G(\mathbf{q}_\parallel)v_{2D}N_s\chi^0] .\end{aligned} \tag{3.18}$$

We emphasize that, within our GRPA, this is an exact result. No plasmon pole approximation has been made. In the RPA, where $G(\mathbf{q}_\parallel)$ is set to zero, (3.18) reduces to

$$v_{aa}^{\rm eff}(\mathbf{q},\omega)=\frac{v_+}{2(1-v_+N_s\chi^0)}+\frac{v_-}{2(1-v_-N_s\chi^0)} . \tag{3.19}$$

For completeness, we note that

$$v_{ba}^{\rm eff}(\mathbf{q},\omega)=\frac{\bar{v}^*}{|2\bar{v}|}\left(\frac{v_+'}{\epsilon_+'}-\frac{v_-'}{\epsilon_-'}\right) . \tag{3.20}$$

As we shall see later, this leads to an effective interaction between electrons in different sheets in a given cell which is quite different from the intrasheet-induced interaction as determined by (3.18).

IV. PLASMON BRANCHES IN SUPERLATTICES: LONG-WAVELENGTH LIMIT

In this section, working mainly in the long-wavelength limit, we examine the new kinds of superlattice plasmons which arise when we have two and three sheets/unit cell. For simplicity, we shall work with the RPA formulas of Sec. II.

For a single sheet/unit cell the dispersion relation is given by (2.11). The structure of (2.11) has been studied extensively in the semiconductor literature, usually with the high-frequency approximation

$$\chi_2^0(\mathbf{q}_\parallel,\omega)=\frac{N'q_\parallel^2}{m^*\omega^2} , \tag{4.1}$$

where N' is the number of electrons in a sheet. In the long-wavelength limit ($\tilde{v}=v$), the zeros of (2.11) are given by

$$\omega_+^2=\omega_{pl}^2\left(\frac{q_\parallel^2}{q_\parallel^2+q_z^2}\right) , \tag{4.2}$$

where $\omega_{pl}^2\equiv 4\pi n_B e^2/m^*$ and $n_B=N'/Ac$ is the effective *bulk* charge density. This plasmon spectrum is acoustic for $q_z\neq 0$, with an effective velocity given by (ω_{pl}/q_z).

The minimum velocity (i.e., the lowest-energy acoustic plasmon) corresponds to a charge fluctuation of opposite sign in alternate sheets.[13] In this case, the low-q result (4.2) is not valid and we must start with (2.11). For $q_\parallel c\ll 1$, calculation gives

$$\omega^2(q_z=\pi/c)=\frac{4\pi ne^2c}{m^*}q_\parallel^2\equiv v^2q_\parallel^2 . \tag{4.3}$$

Since the 2D Fermi velocity is related to the density by $v_{2F}^2=2\pi n/(m^*)^2$, we conclude that

$$\frac{v_{2F}^2}{v^2}=\frac{m}{m^*}\left(\frac{a_0}{2c}\right) , \tag{4.4}$$

where $a_0=1/(me^2)=0.52$ Å is the Bohr radius. In the high-T_c oxide superconductors, one has typically $c\approx 10$–15 Å and thus we conclude that $v_{2F}\ll v$. That is to say, the lowest-energy acoustic plasmon in a superlattice with a single sheet/unit cell is still far *above* the particle-hole continuum, which starts at $v_{2F}q_\parallel$. We conclude that while the $q_z\neq 0$ modes form a band of acoustic plasmons, they are of comparatively high energy.

We next turn to the case of two sheets/unit cell and discuss the zeros of ϵ as given by (2.10). As we noted in earlier sections for the case of two identical sheets, the two

kinds of plasmons $\omega_\pm$ are given by the zeros of $\epsilon_\pm$. These correspond to the solutions of

$$\frac{1}{v_+(\mathbf{q})} = N_s\chi_2^0(\mathbf{q}_\parallel,\omega_+)\,, \tag{4.5}$$

$$\frac{1}{v_-(\mathbf{q})} = N_s\chi_2^0(\mathbf{q}_\parallel,\omega_-)\,. \tag{4.6}$$

These are obvious generalizations of the case for one sheet/unit cell. These modes reduce to the ones given in the literature[12] when one uses the high-frequency approximation (4.1) for χ_2^0. Especially for the ω_- solution, it is better to use a more accurate approximation for the 2D Lindhard function. In the long-wavelength limit $q \ll k_F$, this is given by

$$\frac{1}{A}\mathrm{Re}\chi_{2i}^0(\mathbf{q}_\parallel,\omega) = \begin{cases} N_{2F}(i)\left[\dfrac{\omega}{[\omega^2 - v_{2F}^2(i)q_\parallel^2]^{1/2}} - 1\right], & \omega > v_{2F}(i)q_\parallel, \\ -N_{2F}(i)\,, & \omega < v_{2F}(i)q_\parallel, \end{cases} \tag{4.7}$$

$$\frac{1}{A}\mathrm{Im}\chi_{2i}^0(\mathbf{q}_\parallel,\omega) = \begin{cases} N_{2F}(i)\dfrac{\omega}{[v_{2F}^2(i)q_\parallel^2 - \omega^2]^{1/2}}, & \omega < v_{2F}(i)q_\parallel, \\ 0\,, & \omega > v_{2F}(i)q_\parallel\,. \end{cases} \tag{4.8}$$

Here $N_{2F}(i)$ is the density of states at the 2D Fermi surface of sheet i and $v_{2F}(i)$ is the associated Fermi velocity. In a 2D free electron gas, we recall that $N_2(\epsilon_F) = m^*/\pi$ and $n = k_F^2/2\pi$, where n is the electronic surface density N'/A. In this long-wavelength limit, the particle-hole continuum extends to $v_{2F}q_\parallel$.

A graphical solution of (4.6) using (4.7) shows that the ω_- solution is pulled down in energy compared to the solution of (2.11) which for small q reduces to

$$\frac{1}{v(\mathbf{q})} = N_s\chi_2^0(\mathbf{q}_\parallel,\omega)\,. \tag{4.9}$$

Since $v_-(\mathbf{q}) \to 0$ in the long-wavelength limit, it is clear that $\omega_-(\mathbf{q})$ will be close to $v_{2F}q_\parallel$. In contrast, the ω_+ solution of (4.5) is shifted to higher energies, approaching the plasmon branch given by (4.2) in the $q \to 0$ limit (except that n_B is now $2N/Ac$, since there is now two sheets/unit cell).

Working out the full-density-response function[11] for two identical sheets, we find

$$\chi_{nn}(\mathbf{q}) = \frac{2N_s\chi_2^0}{\epsilon_+\epsilon_-}[1 - N_s\chi_2^0(\tilde{v} - \mathrm{Re}\bar{v})]\,. \tag{4.10}$$

For $q_z = 0$, $\bar{v}$ is real and the ϵ_- factor in the denominator on the right-hand side of (4.10) *cancels* a similar factor in the numerator, leaving

$$\chi_{nn}(\mathbf{q}) = \frac{2N_s\chi_2^0}{\epsilon_+(\mathbf{q}_\parallel, q_z = 0)}\,. \tag{4.11}$$

That is, for $q_z = 0$, only the $\omega_+(q_z = 0)$ mode is a pole of the full-density-response function. The $\omega_-(q_z = 0)$ mode cancels out completely. This result is valid for arbitrary values of d_1 (such that $0 < d_1 < c$) and for any $\mathbf{q}_\parallel$.

Further insight into the two-plasmon mode solutions $\omega_\pm$ of (4.5) and (4.6) is obtained by considering the special limit when $d_1 \Longrightarrow c/2$. In this case,[12] the plasmons must reduce to those of a superlattice of reduced spacing $c/2$. Calculation shows $\bar{v}$ is real for $d_1 = c/2$ and thus $\chi_{nn}(\mathbf{q})$ is once again given by (4.11) but now for arbitrary q_z. That is, the $\omega_-(q_z)$ mode (zero of ϵ_-) exactly cancels out of $\chi_{nn}(\mathbf{q})$. However, we recall that the allowed values of q_z are determined by the Brillouin zone and hence the G_z spectrum. One may show that

$$v_+(\mathbf{q}) = 2\sum_{G_z}{}' \frac{4\pi e^2}{q_\parallel^2 + (q_z + G_z)^2}\,, \tag{4.12}$$

where the sum is now restricted to $G_z = (\mathrm{even})2\pi/c$. We see that effectively the reciprocal-lattice vectors are given by $n2\pi/d_1$. Thus the BZ for the $\omega_+(q_z)$ mode is now expanded from π/c to π/d_1 and this accounts for the "missing" ω_- modes when $d_1 = c/2$.

The preceding results are general in that no specific approximation for χ_2^0 was really needed. For illustrative purposes, we now consider the $\omega_\pm$ branches using the long-wavelength limit given by (4.7). The solutions of (4.5) and (4.6) are found to be given by

$$\omega_\pm^2 = v_{2F}^2q_\parallel^2\frac{(1 + a_\pm)^2}{1 + 2a_\pm}\,, \tag{4.13}$$

where $a_\pm \equiv v_\pm m^*/\pi c$. For $q_\parallel c \ll 1$, one finds

$$v_+ \simeq 2v(\mathbf{q})\,, \quad v_- \simeq 2\pi e^2 d_1(c - d_1)\,. \tag{4.14}$$

The expression for v_- is valid for $q_z = 0$ and $q_z = \pi/c$. For the cases of interest, $a_\pm \gg 1$ and we obtain from (4.13)

$$\omega_+^2(\mathbf{q}) = 2\omega_{pl}^2\frac{q_\parallel^2}{q_\parallel^2 + q_z^2}\,, \tag{4.15}$$

$$\omega_-^2(\mathbf{q}) = v_{2F}^2q_\parallel^2\left[m^*e^2d_1\frac{(c - d_1)}{c}\right]. \tag{4.16}$$

We see that the ω_- branch occurs at a much lower fre-

quency than the ω_+ branch. Numerical calculations in Sec. V for arbitrary values of $\mathbf{q}_\parallel$ and q_z show that in fact the $\omega_-(\mathbf{q})$ branch is almost independent of q_z for $d_1 \ll c$ and is essentially identical to the acoustic plasmon ω_- mode of an isolated bilayer.[22] This corresponds to the $c \to \infty$ limit (in which case, only the $q_z = 0$ mode remains) of our superlattice model. We refer to Sec. V for further discussion.

We next turn to the case of a trilayer unit cell composed of two identical outer sheets (at $z_a = 0$ and $z_c = 2d_1$) and a different sheet at $z_b = d_1$. Apparently such a trilayer basis has never been studied in the semiconductor superlattice literature. The trilayer superlattice RPA dielectric function $\epsilon(\mathbf{q},\omega)$ derived in Ref. 11 reduces to

$$\epsilon(\mathbf{q},\omega) = 1 - N_x\tilde{v}(2\chi^0_{2a} + \chi^0_{2b}) + (N_s\chi^0_{2a})^2[\tilde{v}^2 - |\bar{v}(2d_1)|^2] + 2(N_s\chi^0_{2a})(N_s\chi^0_{2b})[\tilde{v}^2 - |\bar{v}(d_1)|^2]$$
$$+ (N_s\chi^0_{2a})^2(N_s\chi^0_{2b})\{2\tilde{v}|\bar{v}(d_1)|^2 + \tilde{v}|\bar{v}(2d_1)|^2 - \tilde{v}^3 - 2\mathrm{Re}[\bar{v}(2d_1)\bar{v}^*(d_1)\bar{v}^*(d_1)]\}\,. \tag{4.17}$$

In discussing the three plasmon zeros of $\epsilon(\mathbf{q},\omega)$, for simplicity we consider the $c \to \infty$ limit. In actual fact, we shall see that two of these modes involve charge fluctuations which are weakly coupled to those in other cells and thus they are essentially identical (assuming $d_1 \ll c$) to those of an isolated trilayer. In this limit, (4.17) can be reduced to [using (2.17)]

$$\epsilon(\mathbf{q},\omega) = 1 - 2x_a + x_b + x_a^2(1 - e^{-4d_1 q_\parallel}) + 2x_a x_b(1 - e^{-2d_1 q_\parallel}) - x_a^2 x_b(1 - e^{-2d_1 q_\parallel})^2\,, \tag{4.18}$$

where we have defined $x_i \equiv N_s\chi^0_{2i}(\mathbf{q}_\parallel,\omega)v_{2D}(\mathbf{q}_\parallel)$. This can be written in the form given by Mahan and Wu[21]

$$\epsilon(\mathbf{q},\omega) = \epsilon_{a-}(\epsilon_{a+} - x_b\epsilon_{a-})\,, \tag{4.19}$$

where $\epsilon_{a\pm}$ is defined in (3.12) with

$$v_\pm = v_{2D}(1 \pm e^{-2d_1 q_\parallel})\,. \tag{4.20}$$

The first factor in (4.19) corresponds to a plasmon mode in which the two outer sheets have out-of-phase charge fluctuations while the center sheet is undisturbed. We shall denote this as the ω_- plasmon mode, in analogy with the mode which occurs in a bilayer. In the long-wavelength limit $d_1 q_\parallel \ll 1$, the dispersion relation of this ω_- mode is given by

$$x = \frac{1}{2q_\parallel d_1} \quad \text{or} \quad \omega_-^2 = v_{2F}^2 q_\parallel^2(m^* e^2 2d_1)\,, \tag{4.21}$$

exactly the same as the ω_- mode in the case of two layers separated by $2d_1$ [see (4.16)].

The second factor on the right-hand side of (4.19) has two zeros. They are easily found in the $q_\parallel d_1 \ll 1$ limit if we assume all three sheets are identical. One corresponds to

$$x = \tfrac{1}{3} \quad \text{or} \quad \omega_+^2 = 3\left(\frac{2\pi n_s e^2}{m^*}q_\parallel\right). \tag{4.22}$$

This is the ω_+ plasmon mode of a *trilayer* in which the charge fluctuations in all three sheets are in-phase. In actual fact, the coupling of the unit cell in a superlattice dramatically renormalizes this mode. In the long-wavelength limit, the true ω_+ mode is given by the solution of ($\tilde{v} = \bar{v} = v$)

$$\epsilon(\mathbf{q},\omega) \simeq 1 - 3N_s\chi^0_2 v(\mathbf{q})\,. \tag{4.23}$$

The solution of this is identical to (4.2) except the effective charge density is not multiplied by 3. This plasmon corresponds to a charge fluctuation in all three sheets which are in-phase. The other zero of the second factor in (4.19) given by

$$x = \frac{3}{2d_1 q_\parallel} \quad \text{or} \quad \omega_3^2 = v_{2F}^2 q_\parallel^2(\tfrac{2}{3}m^* e^2 d_1)\,. \tag{4.24}$$

This mode corresponds to charge fluctuations on the middle sheet oscillating out-of-phase with those of the two side sheets.

It is these low-energy acoustic plasmons ω_- and ω_3 which are the new feature of a superlattice with a basis of three sheets/unit cell. When the spacing between the sheets (d_1) is much less than the superlattice period c, they are well approximated by the analogous modes of a single trilayer. These features will be in evidence in the numerical results we present in Sec. V. In contrast, the high-energy plasmon branch[13] ω_+ is strongly renormalized by the Coulomb coupling between neighboring cells in the superlattice. We also note that the three plasmon bands will merge into one as $d_1 \to c/3$.

As discussed in Ref. 11, Eq. (4.17) can be used to discuss the plasmons in Y-Ba-Cu-O by taking the middle b layer to be a plane of 1D metallic chains (along y axis). In that case $N_s\chi^0_{2b}(\mathbf{q}_\parallel,\omega) \to N_c\chi^0_1(q_y,\omega)$, where χ^0_1 is the Lindhard response function for a 1D electron gas and N_c is the number of chains/unit volume. There is always a mode corresponding to out-of-phase charge fluctuations in the outer sheets, uncoupled from the middle layer.[21] In Ref. 10, we only discussed the long-wavelength plasmon modes given by the zeros of

$$\epsilon = 1 - (2N_s\chi^0_{2a} + N_c\chi^0_1)v(\mathbf{q})\,. \tag{4.25}$$

In the case of an isolated trilayer[21] described by (4.19), this means we did not discuss the acoustic plasmon zero of ϵ_{a-} but only the zeros of the second factor [which reduces to (4.25) in the long-wavelength limit].

V. PLASMON DISPERSION RELATIONS AND EFFECTIVE ELECTRON INTERACTION: NUMERICAL RESULTS

In this section, we present some numerical results for the zeros of $\epsilon(\mathbf{q},\omega)$ for the case of two and three metallic sheets/unit cell. In the GRPA using the approximation discussed in Sec. III, the dielectric function for a superlattice with *three* sheets at ($z_a=0$, $z_b=d_1$, and $z_c=d_2$) is given by

$$\epsilon_3(\mathbf{q},\omega)=\epsilon_c'(\epsilon_a'\epsilon_b'-N_s\chi_a^0N_s\chi_b^0|\bar{v}(d_1)|^2)-\epsilon_b'N_s\chi_c^0N_s\chi_a^0|\bar{v}(d_2)|^2-\epsilon_a'N_s\chi_c^0N_s\chi_b^0|\bar{v}(d_2-d_1)|^2$$
$$-N_s\chi_a^0N_s\chi_b^0N_s\chi_c^0 2\mathrm{Re}[\bar{v}(d_2)\bar{v}^*(d_1)\bar{v}^*(d_2-d_1)]\,, \tag{5.1}$$

where ϵ_i' is defined in (3.8). This is a natural generalization of the RPA result given in Sec. IV. For *two* sheets (a and b), it reduces to the result given in (3.7), which we will denote by ϵ_2. In our calculations, we use the exact expression for the Lindhard function of a 2D electron gas. In addition, the charge density is chosen to be the same in each sheet, $n_s=1.5\times10^{14}/\mathrm{cm}^2$. This is the sort of value appropriate to oxide superconductors.

Figure 1 shows the zeros of the real part of ϵ_2 for two identical sheets separated by $d_1=3$ Å and a superlattice period of $c=15$ Å, using the RPA. One has two plasmon branches $\omega_\pm(\mathbf{q}_\parallel,q_z)$ corresponding to the zeros of $\epsilon_\pm\equiv1-v_\pm N_s\chi^0$. For a given wave vector $\mathbf{q}_\parallel$, there are N plasmon modes in each branch labeled by $q_z(-\pi/c<q_z<\pi/c)$. In fact, one finds that the $\omega_-(\mathbf{q}_\parallel,q_z)$ mode are essentially degenerate, with almost no dependence on q_z. This is because the ω_- mode involves out-of-phase charge fluctuations in the two sheets in a given unit cell. As a result, there is essentially no *net* charge fluctuation which can couple into the other superlattice unit cells. This becomes more pronounced as the separation d_1 becomes much smaller than $c/2$, as it is in the oxide superconductors. As d_1 increases towards $c/2$, in contrast, the ω_- branch broadens into a band and the "energy gap" between the ω_+ and ω_- branches disappears (see also Ref. 12).

As one example which might be relevant to Y-Ba-Cu-O superconductors,[21] if we ignore effect of the CuO chains (see, however, Ref. 11), one has two CuO_2 sheets separated by $d\simeq3.4$ Å in a superlattice unit cell with $c=11.7$ Å. To the extent that we can ignore charge fluctuations in the BiO and TlO bilayers, the 2:2:1:2 materials may also be viewed as superlattices with two CuO_2 sheets/unit cell. In Bi 2:2:1:2, we have $c=15.4$ Å and $d_1=3.2$ Å; in Tl 2:2:1:2, $c=14.7$ Å and $d_1=3.16$ Å. Thus in both cases, we have $d_1/c\sim1/5$ [as in Fig. 1]. In the first paper in Ref. 12, numerical plots are given for the $\omega_\pm$ plasmon branches [for $d_1/c=1/3$, see Fig. 3; for $d_1/c=1/4$, see Fig. 5; for these ratios, the $\omega_-(\mathbf{q}_\parallel,q_z)$ modes form a band of finite width].

In Fig. 2, we show the plasmon-dispersion dispersion relations as given by the GRPA dielectric function (3.7) in conjunction with (3.2). As expected, both plasmon branches $\omega_\pm$ disappear into the particle-hole continuum at a much lower value of the wave vector $q_\parallel$.

We next turn to three equally spaced identical sheets/unit cell ($d_2=2d_1$) with $d_1=3$ Å and $c=18$ Å. These numbers are appropriate as a model for the 2:2:2:3 superconductors. As shown in Fig. 3, there are now three plasmon branches. Again, because $d_1\ll c$, the two low-frequency plasmon branches are well separated off from the high-frequency ω_+ band and are essentially independent of q_z. The higher branch is the analogue of the ω_- mode in Fig. 1. The new branch (which we label by ω_3) is lower than the ω_- plasmon. In Fig. 4, we show the analogous modes in the hypothetical case where $c=40$ Å. The ω_3 mode is unchanged while the ω_- band sharpens up and loses all dependence on q_z as expected.

In Fig. 5, we plot the real part of $\epsilon_2(\mathbf{q},\omega)$ as a function of ω for two identical sheets (as in Fig. 1). The fact that

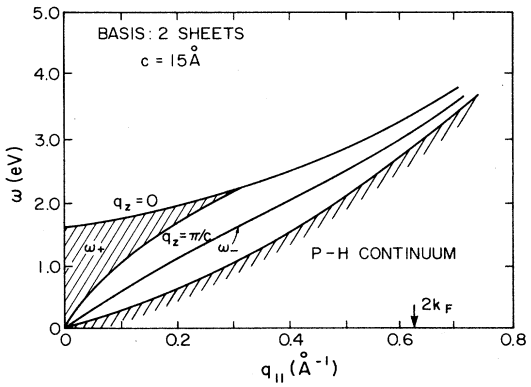

FIG. 1. Plasmon modes $\omega_\pm(\mathbf{q}_\parallel,q_z)$ as a function of the wave vector $q_\parallel$, for a superlattice (period $c=15$ Å) with a basis of two identical sheets (separated by $d_1=3$ Å). In all figures, the sheet density of electrons is $n_s=1.5\times10^{14}/\mathrm{cm}^2$. In Figs. 1–4, we plot the plasmon modes for both $q_z=0$ and $z_z=\pi/c$. The ω_- modes have almost negligible dependence on q_z. These results are based on the RPA results in (4.5) and (4.6) and should describe the CuO_2 planes in 2:2:1:2: superconductors.

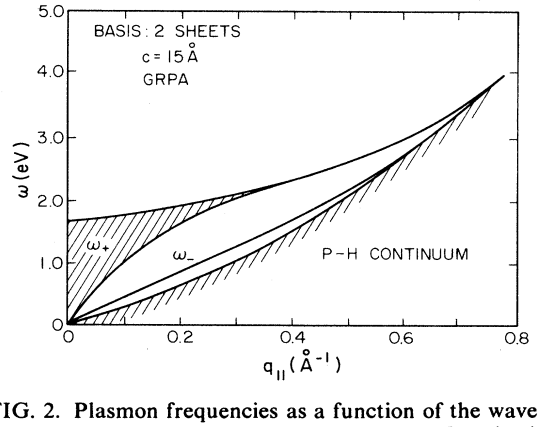

FIG. 2. Plasmon frequencies as a function of the wave vector $q_\parallel$. Same as in Fig. 1 except that GRPA is used [see (3.7)].

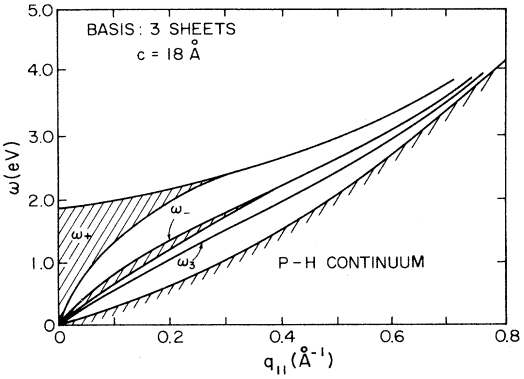

FIG. 3. Three plasmon branches as a function of the wave vector $q_{\|}$, for a superlattice (period $c=18$ Å) with a basis of three identical sheets (separated by $d_1=3$ Å). These results are based on the RPA dielectric function (4.17). The plasmon modes for $0<q_z<\pi/c$ form a band. These results should describe the CuO_2 planes in 2:2:2:3 superconductors.

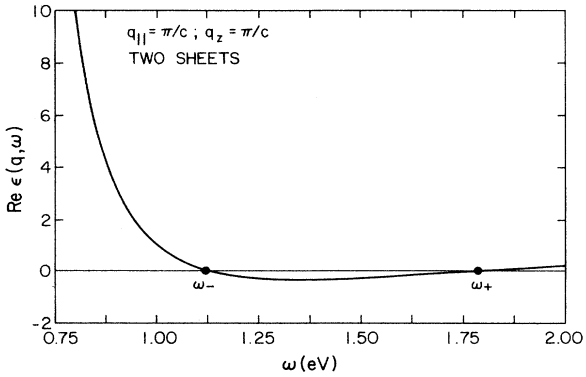

FIG. 5. The real part of the dielectric function $\epsilon(\mathbf{q},\omega)$ for the superlattice described in Fig. 1. In Figs. 5–7, we take $q_{\|}=q_z=\pi/c$.

ϵ_2 is only negative between ω_- and ω_+ is easily understood using the factorized form $\epsilon_2=\epsilon_+\epsilon_-$, where $\epsilon_\pm$ is defined by (3.12) and $v_\pm=\tilde{v}\pm|\bar{v}|$. A similar plot of the real part of $\epsilon_3(\mathbf{q},\omega)$ for three identical sheets (as in Fig. 3) is shown in Fig. 6. In both figures, the particle-hole spectrum (for $q_{\|}=\pi/c$) starts at 0.67 eV.

In the RPA, the effective interaction in a superlattice with a basis of two identical sheets are given in (2.9),

$$v_{aa}^{\rm eff}(\mathbf{q},\omega)=\frac{\tilde{v}-(\tilde{v}^2-|\bar{v}|^2)N_s\chi^0}{\epsilon_2}=\frac{1}{2}\left[\frac{v_+}{\epsilon_+}+\frac{v_-}{\epsilon_-}\right]. \tag{5.2}$$

In Fig. 7, we plot this potential (normalized to $\tilde{v}$). It is attractive for frequencies just below ω_+ and below ω_-, in spite of the behavior of $\mathrm{Re}\epsilon_2$ in Fig. 5. By way of contrast, $v_{ba}^{\rm eff}$ given by (2.9) in the RPA limit is quite different.

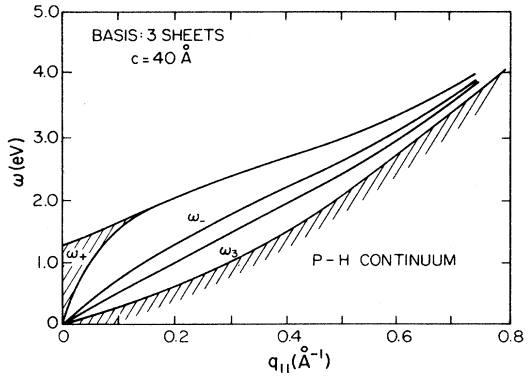

FIG. 4. Plasmon modes in a superlattice with a period of 40 Å and a basis of three identical sheets ($d_1=3$ Å). In comparison with Fig. 3, the plasmon bands are much more narrow, as expected.

From Fig. 5, we see that it will be only attractive in the region $\omega_-<\omega<\omega_+$.

The preceding numerical results suggest that because the spacing between the CuO_2 sheets is so much less than the superlattice period c, the low-frequency plasmon branches are essentially identical to those of an isolated bilayer (see, for example, Ref. 22) or trilayer. In contrast, the high-frequency plasmon branch ω_+ can be treated as if the spacing of the sheets in a unit cell was effectively zero. That is, the ω_+ plasmon branch is the same as for a superlattice with only one sheet/unit cell but with a charge density either two (bilayer) or three (trilayer) times larger.

Using this simplification in the case of two sheets/unit cell, we can easily derive an *analytic* expression for the effective intrasheet electron-electron interaction $v_{aa}^{\rm eff}$ using (3.16) and (2.15). For the ϵ'_+ pole, we use the $d_1=0$ approximation, in which case

$$v'_+=2\tilde{v}(q)-G(q_{\|})v_{2D}=v_{2D}\left[\frac{2\sinh q_{\|}c}{\cosh q_{\|}c-\cos q_z c}-G(q_{\|})\right], \tag{5.3}$$

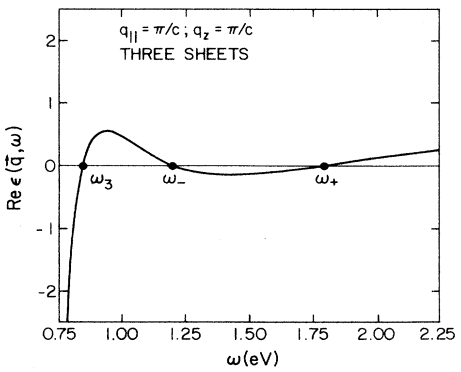

FIG. 6. The real part of $\epsilon(\mathbf{q},\omega)$ for the superlattice described in Fig. 3.

while for the ϵ'_- pole, we use the $c=\infty$ approximation and hence

$$v'_- = v_{2D}[1-e^{-q_\parallel d_1}-G(q_\parallel)] . \tag{5.4}$$

One finds after some calculation that the contribution of the ϵ'_+ branch to $v_{aa}^{\rm eff}(l-l'=0)$ is given by

$$v_+^{\rm eff}(l-l'=0;\mathbf{q}_\parallel,\omega) = \frac{1}{2}\frac{v_{2D}\sinh q_\parallel c\,\mathrm{sgn}(\mathrm{Re}b')}{\sqrt{b'^2-1}} + \frac{1}{2}\frac{(v_{2D}G)^2 N_s\chi^0}{1+v_{2D}GN_s\chi^0} , \tag{5.5}$$

where

$$b' \equiv \cosh q_\parallel c - \frac{2v_{2D}N_s\chi^0(\mathbf{q}_\parallel,\omega)\sinh q_\parallel c}{1+v_{2D}G(q_\parallel)N_s\chi^0(\mathbf{q}_\parallel,\omega)} . \tag{5.6}$$

This reduces to the RPA result obtained in Ref. 17 when we set $G(\mathbf{q}_\parallel)=0$. We note that the region $-1<b'<1$ corresponds to the ω'_+ plasmon band ($b'=1$ corresponds to $q_z=0$ and $b'=-1$ corresponds to $q_z=\pi/c$). In (5.5), we have a negative-square-root singularity for $b'<-1$ and thus an effective interaction which is attractive for $\omega<\omega'_+(\mathbf{q}_\parallel,q_z=\pi/c)$.

The analogous contribution of the ϵ'_- pole in (3.18) based on (5.4) is given by

$$v_-^{\rm eff}(l-l'=0;\mathbf{q}_\parallel,\omega) = \frac{1}{2}\frac{v_{2D}(1-e^{-q_\parallel d_1})+N_s\chi^0(v_{2D})^2[1-e^{-q_\parallel d_1}-G(q_\parallel)]}{1-v_{2D}[1-e^{-q_\parallel d_1}-G(q_\parallel)]N_s\chi^0} . \tag{5.7}$$

This is identical to the contribution of the low-frequency ω'_- plasmon of an isolated bilayer in the GRPA. We note that $v^{\rm eff}$ is negative (attractive) for $\omega<\omega'_-(q_\parallel)$.

Of course, rather than using the approximate analytic forms (5.5) and (5.7), one can always use the full GRPA expression given in (3.18) and carry out the q_z integration in (2.15) numerically.

Similar results can be obtained, using (3.15) in (2.16), for the contribution of the $\omega'_\pm$ plasmons to the induced interaction between electrons in different sheets of the same unit cell.

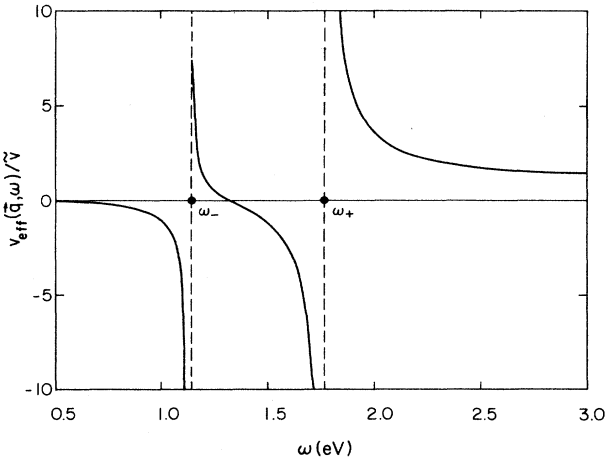

FIG. 7. The effective RPA interaction $\mathrm{Re}v_{aa}^{\rm eff}$ in (5.2) between electrons, as a function of the frequency, for the superlattice described in Fig. 1. The results are normalized with respect to $\tilde{v}(\mathbf{q})$ given in (2.6), the value it would have without any coupling to charge fluctuations. $\mathrm{Re}v_{aa}^{\rm eff}$ is very small but positive for $\omega\leq 0.5$ eV.

VI. CONCLUDING REMARKS

In this paper, we have given a detailed discussion of the plasmon modes in a *superlattice* with a basis of two or three metallic sheets. As we argued in an earlier paper,[11] this model seems appropriate for the oxide superconductors. In the present work, we have gone past the usual RPA and have included local-field effects due to exchange and correlation (in a simple Hubbard approximation). More generally, we have emphasized that if one has n metallic sheets/unit cell, one will have $n-1$ low-energy (essentially acoustic) plasmon branches for a given wave vector $\mathbf{q}$. These are in addition to the high-energy plasmon branch,[13] which involves strong coupling between neighboring cells in the superlattice. Our numerical studies show very dramatically that if the spacing between the sheets (d_1) is much smaller than the superlattice period (c), the $n-1$ low-energy plasmon modes involve charge fluctuations in a given cell which are only weakly coupled to other cells. Thus they can be described using an isolated cell of n layers (such as a bilayer or trilayer).

Clearly our treatment of the band structure of the electrons in a given CuO_2 sheet needs improvement. However, the physics we have tried to emphasize is that arising from the Coulomb coupling of charge fluctuations in different sheets. When a better theory of the charge fluctuations in a given CuO_2 sheet becomes available, it can be incorporated into our analysis.[11] One can easily generalize our results to metallic sheets with two components or bands (see Fetter in Ref. 13).

The most relevant previous work on the plasmon-induced electron-electron interaction worked strictly within the RPA and was concerned with either a superlattice with a single sheet/unit cell,[17] an isolated bilayer,[20] or an isolated trilayer.[21] Our work reduces to the results of Refs. 17 and 21 in the appropriate limits.

The direct observation of the acoustic plasmon branches we have predicted (by high-resolution inelastic electron scattering or some other technique[18]) would be a useful way of confirming the metallic properties of the CuO_2 sheets. In addition, if the Bi_2O_2 or Tl_2O_2 bilayers are metallic (as suggested by band-structure calculations[7-9]), they would give rise to an additional low-energy plasmon mode (see Appendix B for further discussion).

In future work, we hope to use results such as (5.5) and

(5.7) to see how effective superlattice plasmons are for Cooper pairing in the oxide superconductors. In concluding, therefore, we briefly review the current status of plasmon-induced pairing studies. In bulk metals (both 3D and 2D), it is well known that the simple exchange of RPA plasmons by an electron can lead to anomalously large pairing.[24,25] Indeed, it was found[25] that the method used by Takada[24] [the Kirzhnits-Maksimov-Khomskii (KMK) approach to solving Eliashberg's integral equations] gave rise to a considerable underestimate of T_c. However, when one includes vertex corrections in the electron self-energy and goes past the RPA, plasmons are found to be much less effective as a pairing mechanism.[26] In the case of a single 2D metallic sheet, similar results have been recently reported by Canright and Vignale.[19] In particular they found that within the RPA, one obtained strong pairing in the low-density limit, but that this was not the case when one worked with an effective electron-electron interaction given by the GRPA [Eq. (3.11) with $\tilde{v}_a' = v_{2D}(1-G)$].

The question which still remains is whether the situation in superlattices is more conductive to pairing. Comparing the situation with that in conventional superconductors,[27] one can think of the first term in (3.18) as the analog of the dynamically screened Coulomb interaction while the second term is the analog of the lattice phonon-induced interaction. The characteristic frequencies are set by ω_+ and ω_-, respectively. We expect that the high-energy ω_+ plasmon branch[13] will not be an effective-pairing mechanism when one goes past the RPA. Whether the low-energy ω_- plasmon branch is more robust requires more study. At present, two relevant RPA calculations have been reported but the situation is somewhat unclear. Giuliani[20] has discussed plasmon-induced pairing in an *isolated* bilayer but since he made use of the KMK approximation, the results are not definitive. Mahan and Wu[21] have given a detailed discussion for a trilayer (two outer CuO_2 sheets with a middle layer of parallel CuO chains) such as occurs in Y-Ba-Cu-O materials.[10] However they found no pairing in their RPA analysis and, moreover, gave various arguments why one would not expect it in a BCS-plasmon exchange model. This is puzzling since it appears to be in sharp conflict with all of the literature on this topic.[19,20,24-26] Moreover, Mahan and Wu[21] do not give any convincing arguments why the effect of short-wavelength plasmons should be any different than long-wavelength plasmons.

We feel that the GRPA results of the present paper will be useful in extending the calculations of Canright and Vignale,[19] and hopefully help to settle the question whether the low-energy acoustic plasmons which occur in superlattices with a basis are responsible for the high superconducting transition temperatures in the oxides. We note that T_c increases[2-6] with the number of metallic layers/unit cell, as does the number of acoustic plasmons which might give rise to pairing.[28]

ACKNOWLEDGMENTS

We would like to thank Dr. R. Q. Yang of the University of Science and Technology of China (Hefei) for a copy of his work prior to publication. This research was started while A.G. was on sabbatical leave (1987-1988) at Kyoto University and was partially supported by the Japan-Canada Exchange Program through the Japan Society for Promotion of Science and NSERC of Canada. A.G. would also like to thank Professor M. Plischke and the Department of Physics at Simon Fraser University for their hospitality during July of 1988.

APPENDIX A

In the case of a superlattice with a basis of three equally spaced metallic sheets ($z_a=0$, $z_b=d_1$, and $z_c=2d_1$), one finds the effective electron interactions satisfy the coupled RPA equations

$$\begin{aligned}
&\epsilon_a v_{aa}^{\rm eff} - \bar{v}(d_1)N_s\chi_b^0 v_{ba}^{\rm eff} - \bar{v}(2d_1)N_s\chi_c^0 v_{ca}^{\rm eff} = \tilde{v}\,,\\
&-v_{aa}^{\rm eff}\bar{v}^*(d_1)N_s\chi_a^0 + \epsilon_b v_{ba}^{\rm eff} - \bar{v}(d_1)N_s\chi_c^0 v_{ca}^{\rm eff} = \bar{v}^*(d_1)\,,\\
&-v_{aa}^{\rm eff}\bar{v}^*(2d_1)N_s\chi_a^0 - \bar{v}^*(d_1)N_s\chi_b^0 v_{ba}^{\rm eff} + \epsilon_c v_{ca}^{\rm eff} = \bar{v}^*(2d_1)\,.
\end{aligned} \tag{A1}$$

These are the equivalent to Eq. (2.8) for a bilayer basis, and similar notation is used. Solving these coupled equations, one finds, for example,

$$\begin{aligned}
v_{aa}^{\rm eff}(\mathbf{q},\omega) = \{&\tilde{v} - N_s\chi_b^0[\tilde{v}^2 - |\bar{v}(d_1)|^2] - N_s\chi_c^0[\tilde{v}^2 - |\bar{v}(2d_1)|^2]\\
&+ N_s\chi_b^0 N_s\chi_c^0[\tilde{v}^3 - 2|\bar{v}(d_1)|^2\tilde{v} - |\bar{v}(2d_1)|^2\tilde{v} + 2\,{\rm Re}\bar{v}(2d_1)\bar{v}^*(d_1)\bar{v}^*(d_1)]\}/\epsilon_3\,,
\end{aligned} \tag{A2}$$

where ϵ_3 is the RPA superlattice dielectric function for this system. For the special case of $\chi_a^0=\chi_c^0$, ϵ_3 reduces to the expression given in (4.17). If we further work in the $c\to\infty$ limit (i.e., the trilayers are isolated), $\tilde{v}$ and $\bar{v}$ are given by (2.17). In this case, (A2) can be shown to simplify to the expression S_{22} given by Mahan and Wu.[21]

APPENDIX B

Let us consider a superlattice model for the 2:2:1:2-Bi superconductor where the superlattice unit cell is viewed as having a single Bi_2O_2 metallic bilayer and two CuO_2 sheets. To the extent that we work in the long-wavelength limit, the dielectric function simplifies to the first two terms on the right-hand side of (4.17). Generalizing to n CuO_2 sheets/unit cell for $Bi_2Sr_2Ca_{n-1}O_{4+2n}$, the zeros of ϵ are given by the solutions of ($qc \ll 1$)

$$\frac{1}{v(\mathbf{q})} = N_s[n\chi_{\rm CuO}^0(\mathbf{q}_\parallel,\omega) + \chi_{\rm BiO}^0(\mathbf{q}_\parallel,\omega)]\,, \tag{B1}$$

where, for example, $\chi_{\rm CuO}^0$ is the 2D Lindhard function describing the relavant Landau quasiparticles of a CuO_2 sheet.

It is clear from (4.7) that there are only *two* solutions of (B1), one low-energy superlattice plasmon mode and the usual high energy superlattice plasmon. That is, (B1) does not exhibit the expected $n-1$ additional low-energy plasmon modes. One has to keep the higher-order terms in (B1) to pick up these, as we discussed in Sec. IV for the case of three CuO_2 sheets.

The low-frequency plasmon solution of (B1) will be denoted here by $\omega_3(\mathbf{q})$. From available band-structure studies,[7-9] we have $v_{2F}(\mathrm{CuO}) \ll v_{2F}(\mathrm{BiO})$ and thus the ω_3 plasmon will occur in the window

$$v_{2F}(\mathrm{CuO})q_{\parallel} < \omega_3 < v_{2F}(\mathrm{BiO})q_{\parallel} . \tag{B2}$$

It is useful to make a graphical plot of the right-hand side of (B1). Making use of (4.7), we have for ω in the window given by (B2)

$$\frac{1}{v(q)} = \frac{1}{c}\left[nN_{2F}(\mathrm{CuO})\left(\frac{\omega}{[\omega^2 - v_{2F}^2(\mathrm{CuO})q_{\parallel}^2]^{1/2}} - 1 \right) - N_{2F}(\mathrm{BiO}) \right] . \tag{B3}$$

The solution of this is given by

$$\omega_3(\mathbf{q}) = S(\mathbf{q},n)v_{2F}(\mathrm{CuO})q_{\parallel} , \tag{B4}$$

where

$$s \equiv \left(\frac{f^2}{1-f^2} \right)^{1/2} \tag{B5}$$

and

$$f(\mathbf{q},n) = \frac{q^2 + 4\pi e^2[nN_{2F}(\mathrm{CuO}) + N_{2F}(\mathrm{BiO})]/c}{4\pi e^2 nN_{2F}(\mathrm{CuO})/c} \simeq 1 + \frac{N_{2F}(\mathrm{BiO})}{nN_{2F}(\mathrm{CuO})} . \tag{B6}$$

The last line assumes we are working in the limit $q^2 \ll q_{\mathrm{FT}}^2$, where q_{FT} is effectively the Fermi-Thomas wave vector in this problem. We note $f(\mathbf{q},n)$ decreases as n increases and thus $S(n)$ increases with n. Of course, since $\omega_3(\mathbf{q})$ is in the window (B2), we must have

$$S(\mathbf{q},n) < \frac{v_{2F}(\mathrm{BiO})}{v_{2F}(\mathrm{CuO})} . \tag{B7}$$

We also remark that the $\omega_3(\mathbf{q})$ acoustic plasmon in (B4) is only damped due to coupling with the BiO bilayer particle-hole excitations (i.e., it would be independent of n).

The question of whether the Bi_2O_2 bilayer is metallic is still controversial. The observation of an additional acoustic plasmon branch whose frequency varied with the number of CuO_2 sheets in a unit cell as predicted by (B4)-(B7) is one way of answering this question . In this connection, we note band-structure studies[29] suggest that the Bi_2O_2 bilayer is not metallic in Bi 2:2:0:1 but is metallic in Bi 2:2:1:2 and 2:2:2:3. In connection with a pairing mechanism due to low-energy plasmons,[28] this gives a natural explanation of why T_c is so low in Bi 2:2:0:1 (10 K) as compared with Bi 2:2:1:2 (85 K) and 2:2:2:3 (110 K).

*Permanent address: Computing Services, University of Toronto, Toronto, Ontario, Canada M5S 1A7.

[1]H. Maeda, Y. Tanaka, M. Fukutomi, and T. Asano, Jpn. J. Appl. Phys. **27**, L209 (1988).

[2]S. A. Sunshine, T. Siegrist, L. F. Schneemeyer, D. W. Murphy, R. J. Cava, B. Batlogg, R. B. van Dover, R. M. Fleming, S. H. Glarum, S. Nakahara, R. Farrow, J. J. Krajewski, S. M. Zahurak, J. V. Waszczak, J. H. Marshall, P. Marsh, L. W. Rupp, Jr., and W. F. Peck, Phys. Rev. B **38**, 893 (1988).

[3]J. M. Tarascon, Y. Le Page, P. Barboux, B. G. Bagley, L. H. Greene, W. R. McKinnon, G. W. Hull, M. Giroud, and D. M. Hwang, Phys. Rev. B **37**, 9382 (1988).

[4]J. M. Tarascon, W. R. Mckinnon, P. Barboux, D. M. Huang, B. G. Bagley, L. H. Greene, G. Hull, Y. Le Page, N. Stoffel, and M. Giroud, Phys. Rev. B **38**, 8885 (1988).

[5]S. S. P. Parkin, V. Y. Lee. E. M. Engler, A. I. Nazzal, T. C. Huang, G. Gorman, R. Savoy, and R. Beyers, Phys. Rev. Lett. **24**, 2539 (1988).

[6]R. M. Hazen, L. W. Finger, R. J. Angel, C. T. Prewitt, N. L. Ross, C. G. Hadidiacos, P. J. Heaney, D. R. Veblen, Z. Z. Sheng, A. El Ali, and A. M. Hermann, Phys. Rev. Lett. **60**, 1657 (1988).

[7]S. Massidda, J. Yu, and A. J. Freeman, Physica C **152**, 251 (1988); J. Yu, S. Massidda, and A. J. Freeman, *ibid.* **152**, 273 (1988).

[8]M. S. Hybertsen and L. F. Mattheiss, Phys. Rev. Lett. **60**, 1661 (1988).

[9]H. Krakuer and W. E. Pickett, Phys. Rev. Lett. **60**, 1665 (1988).

[10]A. Griffin, Phys. Rev. B **37**, 5943 (1988).

[11]A. Griffin, Phys. Rev. B **38**, 8900 (1988).

[12]R. A. Mayanovic, G. F. Giuliani, and J. J. Quinn, Phys. Rev. B **33**, 8390 (1986); C. Zhang and N. Tzoar, *ibid.* **34**, 1050 (1986); R. Q. Yang (unpublished).

[13]A. L. Fetter, Ann. Phys. (N.Y.) **88**, 1 (1974); see also, V. Z. Kresin and H. Morawitz, Phys. Rev. B **37**, 7854 (1988) for application to oxide superconductors.

[14]C. Jonson, J. Phys. C **9**, 3055 (1976); G. Vignale, Phys. Rev. B **38**, 811 (1988).

[15]G. D. Mahan, *Many-Particle Physics* (Plenum, New York, 1981), p. 473ff.

[16]H. K. Sy and L. M. Song, Phys. Status Solidi B **136**, 201 (1986).

[17]P. Hawrylak, G. Eliasson, and J. J. Quinn, Phys. Rev. B **37**, 10187 (1988).

[18]J. K. Jain and S. Das Sarma, Surf. Sci. **196**, 466 (1988).

[19]G. S. Canright and G. Vignale, Phys. Rev. B **39**, 2740 (1989). For earlier literature on plasmon-induced pairing in a single sheet, see the review by V. Z. Kresin, J. Mater. Res. **2**, 793 (1987).

[20]G. F. Giuliani, Surf. Sci. **196**, 476 (1988).
[21]G. D. Mahan and J. W. Wu, Phys. Rev. B **39**, 265 (1989).
[22]G. F. Santoro and G. F. Guiliani, Phys. Rev. B **37**, 937 (1988).
[23]This corrects $\bar{v}$ in (25) of Ref. 11.
[24]Y. Takada, J. Phys. Soc. Jpn. **45**, 786 (1978); **49**, 1713 (1980).
[25]H. Rietschel and L. J. Sham, Phys. Rev. B **28**, 5100 (1983).
[26]M. Grabowski and L. J. Sham, Phys. Rev. B **29**, 6132 (1984).
[27]See, for example, the discussion in J. R. Schrieffer, *Theory of Superconductivity* (Benjamin, New York, 1964), Chap. 6. In particular, compare Fig. 6.11 of this reference with Fig. 7 of this paper.
[28]A. Griffin (unpublished).
[29]P. A. Sterne and C. S. Wang, J. Phys. C **21**, L949 (1988).